ELSEVIER

Journal of Organometallic Chemistry 637–639 (2001) 356–363

Journal of Organometallic Chemistry

www.elsevier.com/locate/jorganchem

Complexation and electrochemical sensing of anions by amide-substituted ferrocenyl ligands

Olivier Reynes [a], Frederic Maillard [a], Jean-Claude Moutet [a,*], Guy Royal [a], Eric Saint-Aman [a], Gabriella Stanciu [a], Jean-Pierre Dutasta [b], Isabelle Gosse [b], Jean-Christophe Mulatier [b]

[a] *Laboratoire d'Electrochimie Organique et de Photochimie Rédox, UMR CNRS 5630, Université Joseph Fourier Grenoble I, BP 53, 38041 Grenoble Cedex 9, France*

[b] *Laboratoire de Stéréochimie et Interactions Moléculaires, UMR CNRS 5532, École Normale Supérieure de Lyon, 46 Allée d'Italie, F-69364 Lyon Cedex 07, France*

Received 10 January 2001; received in revised form 15 March 2001; accepted 19 March 2001

Abstract

New amide-containing ferrocenyl ligands, $\mathbf{L_{1-5}}$, were prepared and the voltammetric and ^{1}H NMR investigations of anion binding were carried out in organic media. The electrochemical recognition ability of $\mathbf{L_{1-5}}$ towards F^-, HSO_4^-, $H_2PO_4^-$ and ATP^{2-} is based on the synergy between H-bonding to amide protons in anion complexation to reduced, neutral ligands and ion-pairing interactions developed with the oxidized, cationic form of the ligands. The strength of the anion–ligand interactions depends on the number of ferrocene centers and amide groups in the receptor, and on the accessibility of the binding sites. Clear two-wave cyclic voltammetry features allowed the amperometric titration of $H_2PO_4^-$ and ATP^{2-} by ligands $\mathbf{L_4}$ and $\mathbf{L_5}$ built from a cyclotriveratrylene structural unit, and containing a combination of three ferrocene centers with three ($\mathbf{L_4}$) or six ($\mathbf{L_5}$) amide groups.

Keywords: Ferrocene; Redox-active ligands; Anion complexation; Electrochemical recognition; Cyclotriveratrylene

1. Introduction

The design of molecular receptors having the ability to selectively bind and sense cationic, anionic, or even neutral guests via a macroscopic physical response is an area of intense activity [1,2]. From the first reports in the late 1970s on the synthesis and complexation of metallocene-containing macrocyclic ligands [3,4] capable of electrochemical detection of a metal cation [5], ferrocene has largely proved to be a simple and remarkably robust building block for the construction of redox-responsive receptors [2]. In this context, the design of reagents for anionic sensing is rapidly gaining interest [6,7], stimulated by the importance of small inorganic anions in biochemical processes and from an environmental point of view. Electrochemical sensors containing the ferrocene entity are of particular interest, as they offer the possibility to modulate the anion–receptor interactions according to the redox state; e.g. electrostatic interactions can be switched on by the oxidation of ferrocene to ferricinium. The driving force responsible for the anion-binding ability of these receptors in their neutral ferrocene form is usually the H-bonding interactions between the guest anion and H-bond donor groups appended to the receptor, such as amide [1,2,8] or pyrrole [9] groups. The presence of additional H-bond acceptor groups like amine, pyridine and bipyridine [10–13] in the binding sites enhances the interaction between the receptor and dihydrogenphosphate or hydrogensulphate anions. Another strategy based on hard acid–hard base interaction has been developed for sensing fluoride anion with boronic derivatives of ferrocene [14]. Taking advantage of the dendritic effect, ferrocenyl dendrimers exhibiting anionic electrochemical recognition properties have also been reported [15,16]. The dendritic effect found in the

* Corresponding author. Tel.: +33-4-76514-600; fax: +33-4-76514-267.

E-mail address: jean-claude.moutet@ujf-grenoble.fr (J.-C. Moutet).

0022-328X/01/$ - see front matter
PII: S0022-328X(01)00935-4

electrochemical recognition of small oxo-anions has been demonstrated using poly(amidoferrocene) and poly(aminoferrocinium). Sensing properties of the latter are enhanced through the synergy between $X^- \cdots H-N$ hydrogen bonding, electrostatic attraction in the oxidized state and shape selectivity [15]. Silicon-based ferrocenyl dendrimers containing Si–NH group are able to sense oxo-anions potentiometrically and amperometrically in homogeneous solution, and at the electrode | solution interface after the immobilization of dendrimer onto the electrode surface [16].

In this paper, we present a series of new ferrocenyl ionophores, $\mathbf{L_{1-5}}$ (Chart 1), designed for anionic sensing. They are based on the combination of ferrocene as the signaling unit and secondary amide groups as H-bond donors. $\mathbf{L_{1-5}}$ differ by: (i) the number of ferrocene centers; (ii) the number of amide groups; and (iii) in the preorganization of the binding site.

2. Experimental

2.1. Instrumentation, solvents and reagents

The electrochemical equipment has been described in Ref. [13]. Experiments were conducted in a three-electrode cell under an argon atmosphere and at room temperature (r.t.). The working electrode was a platinum or a carbon disc (5 and 3 mm in diameter, respectively) polished with 1 μm diamond paste. The Ag/10 mM $AgNO_3$ in $CH_3CN + 0.1$ M tetra-*n*-butylammonium perchlorate (TBAP) system was used as a reference electrode. The redox potential of the regular ferrocene/ferricinium (Fc/Fc^+) couple is 0.07 V under our experimental conditions. Acetonitrile (Rathburn, HPLC grade S) was used as received. Dichloromethane was dried over neutral aluminum oxide (activity I) for at least 4 days before use. TBAP (Fluka) was dried under vacuum at 80 °C for 3 days. Tetraethylammonium fluoride, tetra-*n*-butylammonium hydrogensulphate and dihydrogenphosphate were of the highest purity commercially available and were used without further purification. The di(tetra-*n*-butylammonium) salt of adenosine-5′-triphosphate (ATP^{2-}) was obtained from its corresponding disodium salt by ion exchange on Amberlite IRC50 in the $n\text{-}Bu_4N^+$ form.

^{1}H NMR experiments were conducted at 22 °C on a Brucker AC250 spectrometer using the solvent deuterium signal as an internal reference. UV–vis spectra were obtained using a Cary 1 spectrophotometer.

2.2. Redox ligands

Ligands $\mathbf{L_{1-5}}$ were synthesized by the reaction of 1-chlorocarbonylferrocene [17] or 1,1′-bis-chlorocarbonylferrocene [18] with the desired primary amine, i.e. 4-methoxyaniline ($\mathbf{L_1}$, $\mathbf{L_2}$), 1,2-bis(2-aminoethoxy)-benzene ($\mathbf{L_3}$), (±)-3,8,13-triamino-2,7,12-trimethoxy-10,15-dihydro-5*H*-tribenzo[*a*,*d*,*g*]cyclononene [19] ($\mathbf{L_4}$) and (±)-2,7,12-tris(2-aminoethyl carbamoylmethoxy)-3,8,13-trimethoxy-10,15-dihydro-5*H*-tribenzo[*a*,*d*,*g*]-cyclononene [20] ($\mathbf{L_5}$), in dried CH_2Cl_2 containing freshly distilled triethylamine. For $\mathbf{L_{1-3}}$ the stoichiometric mixture was stirred overnight at r.t. under an argon atmosphere, then filtered and evaporated to dryness in vacuo. For the synthesis of $\mathbf{L_3}$, solutions of 1,1′-bis-chlorocarbonylferrocene (0.5 mmol in 50 ml of CH_2Cl_2) and 1,2-bis(2-aminoethoxy)benzene (0.5 mmol in 50 ml of CH_2Cl_2) were added dropwise simultaneously over 4 h in 200 ml of CH_2Cl_2 containing 1 mmol of triethylamine. The mixture was stirred for 24 h. The crude product was extracted with CH_2Cl_2, the organic phase washed with H_2O, and the solvent removed under vacuum. The resulting orange–brown solid was purified

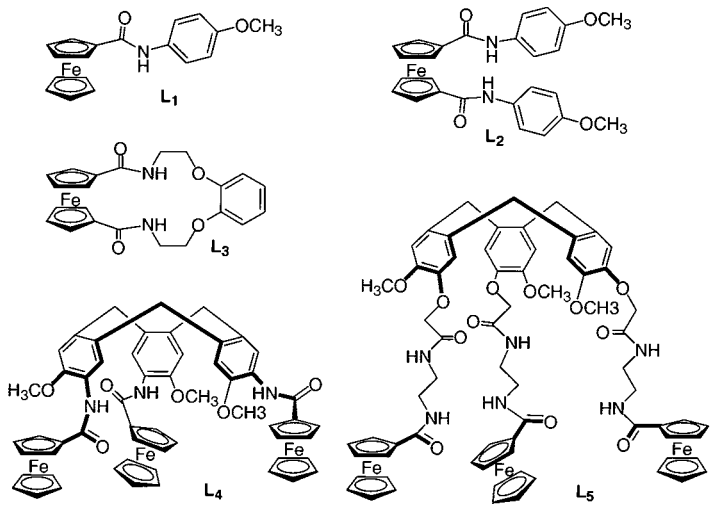

Chart 1. Redox ligands used in this study.

by thin layer chromatography on neutral alumina plates eluted with CH_2Cl_2, to yield $\mathbf{L_1}$ (75%), $\mathbf{L_2}$ (38%) and $\mathbf{L_3}$ (55%) as orange solids. Cyclotriveratrylene-based hosts $\mathbf{L_{4,5}}$ were prepared from their corresponding amine precursors, four equivalents of 1-chloro carbonylferrocene and an excess of triethylamine in CH_2Cl_2. The mixture was stirred overnight at r.t. under an argon atmosphere, and the solvent was removed under vacuum. Crude $\mathbf{L_4}$ was dissolved in CH_2Cl_2 and the organic phase was washed with water, dried over Na_2SO_4 and the solvent removed under vacuum to give $\mathbf{L_4}$ almost quantitatively, which was used without further purification. Crude $\mathbf{L_5}$ was dissolved in a minimum amount of CH_2Cl_2. Diethylether was added until a precipitate was formed. After one night stirring the solid orange compound was recovered by filtration to give $\mathbf{L_5}$ (77%).

$\mathbf{L_1}$. FABMS; m/z (positive mode): 435 $[M+H]^+$; ^{1}H NMR ($CDCl_3$,): δ 3.80 (s, 3H, C*H*$_3$–O), 4.24 (s, 5H, *H*–Cp), 4.40 (m, 2H, H_β–Cp), 4.75 (m, 2H, H_α–Cp), 6.89 (d, 2H, *H*–Ph), 7.29 (s, 1H, N*H*), 7.49 (d, 2H, *H*–Ph); UV–vis: λ (nm) (ε, $M^{-1}\,cm^{-1}$) (d–d band; CH_3CN): 444 (2020).

$\mathbf{L_2}$. FABMS; m/z (positive mode): 484 $[M+H]^+$; ^{1}H NMR ($CDCl_3$): δ 3.76 (s, 6H, C*H*$_3$–O), 4.43 (m, 4H, H_β–Cp), 4.62 (m, 4H, H_α–Cp), 6.88 (d, 4H, *H*–Ph), 7.67 (d, 4H, *H*–Ph), 8.69 (s, 2H, N*H*); UV–vis: λ (nm) (ε, $M^{-1}\,cm^{-1}$) (d–d band; CH_3CN): 433 (2030).

$\mathbf{L_3}$. FABMS; m/z (positive mode): 435 $[M+H]^+$; ^{1}H NMR ($CDCl_3$): δ 3.56–3.62 (m, 4H, –NH–C*H*$_2$), 4.29 (t, 4H, –C*H*$_2$–O–), 4.48 (m, 4H H_β–Cp), 4.53 (m, 4H, H_α–Cp), 6.80 (t, 2H, N*H*), 7.08 (m, 4H, *H*–Ph–); UV–vis: λ (nm) (ε, $M^{-1}\,cm^{-1}$) (d–d band; CH_3CN): 355 (1960).

$\mathbf{L_4}$. FABMS; m/z (positive mode): 1042 $[M+H]^+$; ^{1}H NMR ($CDCl_3$): δ 3.67 (d, 3H, Ph–*CH*$_2$–Ph–), 3.95 (s, 9H, –O–*CH*$_3$), 4.18 (s, 15H, *H*–Cp), 4.35 (m, 6H, *H*–Cp), 4.71 (m, 6H, *H*–Cp), 4.81 (d, 3H, Ph–*CH*$_2$–Ph–), 7.03 (s, 3H, *H*–Ph), 8.01 (s, 3H, *H*–Ph), 8.50 (s, 3H, N*H*); UV–vis: λ (nm) (ε, $M^{-1}\,cm^{-1}$) (d–d band; CH_3CN): 444 (12 550).

$\mathbf{L_5}$. FABMS; m/z (positive mode): 1345 $[M+H]^+$; ^{1}H NMR ($CDCl_3$): δ 3.48 (m, 15H, N–*CH*$_2$*CH*$_2$–N and Ph–*CH*$_2$–Ph), 3.79 (s, 9H, –O–*CH*$_3$), 4.13 (s, 15H, *H*–Cp), 4.29 (m, 6H, *H*–Cp), 4.48 (m, 6H, O–*CH*$_2$–CO–), 4.63 (m, 9H, *H*–Cp and Ph–*CH*$_2$–Ph), 6.60 (br t, 3H, N*H*), 6.77 (s, 3H, *H*–Ph), 6.82 (s, 3H, *H*–Ph), 7.36 (br t, 3H, N*H*); UV–vis: λ (nm) (ε, $M^{-1}\,cm^{-1}$) (d–d band; CH_3CN): 439 (7580).

2.3. Titration procedure and determination of association constants

Electrochemical and ^{1}H NMR titrations were carried out by adding small volumes of concentrated stock solutions of the considered anion to ligand solutions. ^{1}H NMR titration curves were obtained by monitoring variations of H–N and H–Cp chemical shifts in 5–10 mM solutions of redox ligands in CD_3CN or CD_2Cl_2 on the addition of anions in the 0.1–10 molar equivalent range. Association constants K between the reduced neutral ligands $\mathbf{L}$ and anions A^- were determined by considering the formation of 1:1 $\mathbf{LA}^-$ complexes, according to:

$$\mathbf{L} + A^- \rightleftarrows \mathbf{LA}^- \quad (1)$$

with $K = [\mathbf{LA}^-]/([\mathbf{L}][A^-])$.

Assuming a fast exchange at the NMR time scale, the 1:1 binding isotherm can be expressed as Eq. (2)

$$\Delta\delta = ([\mathbf{L}]_t + [A^-]_t + K^{-1} - (([\mathbf{L}]_t + [A^-]_t + K^{-1})^2 - 4[\mathbf{L}]_t[A^-]_t)^{1/2})\,\Delta\delta\max/(2[\mathbf{L}]_t) \quad (2)$$

where $[\,]_t$ denotes the total concentration, and $\Delta\delta_{max}$ the maximal downfield shift of the resonance of the considered proton. Using a non-linear regression method [21], the titration curves $\Delta\delta$ versus $[A^-]_t$ were fitted to the 1:1 binding isotherm giving consistent results in all cases.

3. Results and discussion

3.1. Association of neutral receptors with F^-, $H_2PO_4^-$, ATP^{2-} and HSO_4^-

The association constants K were determined at 295 K in millimolar solutions of ligands in CD_2Cl_2 or CD_3CN, using a standard ^{1}H NMR titration and monitoring the shifts of amide or cyclopentadienyl proton resonances on the addition of increasing amounts of a given anion (see Section 2). Results were analyzed using a non-linear regression method, and by assuming a 1:1 binding isotherm (Table 1). The 1:1 binding isotherm gave consistent fits for all the experimental data. The formation of complexes with higher stoichiometry, e.g. 2:1 anion–ligand ratio, can be reasonably excluded because of the establishment of strong repulsive electrostatic interactions between the two anions in close proximity.

Addition of anions to solutions of $\mathbf{L_1}$, $\mathbf{L_2}$, $\mathbf{L_3}$ and $\mathbf{L_5}$ caused significant perturbations in their ^{1}H NMR spectra. A typical example ($\mathbf{L_5} + ATP^{2-}$) is shown in Fig. 1. However, no changes were observed in the $\mathbf{L_4}$ spectrum when either fluoride or dihydrogenphosphate anion was used. In contrast, the –CO–NH and H_α–Cp resonances in $\mathbf{L_1}$, $\mathbf{L_2}$, $\mathbf{L_3}$ and $\mathbf{L_5}$ are shifted downfield, showing the formation of complexes between these neutral ligands and the surveyed anions.

It is noteworthy that the strongest perturbations were observed for the N–H resonances on complexation with

Table 1
Association constants (K, M^{-1}) between $\mathbf{L_{1-5}}$ and the surveyed anions[a]

	$\mathbf{L_1}$	$\mathbf{L_2}$	$\mathbf{L_3}$ [b]	$\mathbf{L_4}$	$\mathbf{L_5}$
F^- [c]	20 (0.64)	230 (0.48)	110 (0.16)	[d]	69 (0.48)
$H_2PO_4^-$ [e]	40 (2.00)	65 (2.98)	25 (1.56)	[d]	89 (1.80)
ATP^{2-} [e]	[f]	[f]	[f]	[f]	63 (2.13)
HSO_4^- [e]	[f]	[f]	10 (0.52)	[f]	[f]

[a] Determined from ^1H NMR data (see the experimental section), at 295 K in CD_2Cl_2 unless otherwise noted; in parentheses is the maximum downfield shift ($\Delta\delta_{max}$, ppm) for H-amide or H_α–Cp resonances.
[b] In CD_3CN.
[c] $\Delta\delta_{max}$ for the H_α–Cp proton.
[d] Too weak to be determined (no significant change in the NMR spectrum).
[e] $\Delta\delta_{max}$ for the H-amide proton.
[f] Not studied.

$H_2PO_4^-$. For example, the amide protons of $\mathbf{L_1}$ and $\mathbf{L_5}$ are shifted ($\Delta\delta_{max} = 2.0$ and 1.8 ppm) much more than the cyclopentadienyl protons ($\Delta\delta_{max} = 0.23$ and < 0.01 ppm, respectively, for the H_α–Cp protons). This shows that the complexation of the dihydrogenphosphate anion proceeds mainly via H-bonding interactions with the amide protons. In addition, the two resonances for the two non-equivalent amide protons in $\mathbf{L_5}$ are shifted downfield by the same order of magnitude in the presence of $H_2PO_4^-$. This observation indicates that they are both involved in the complexation process. A similar association constant was found for $\mathbf{L_5} + ATP^{2-}$, but $\Delta\delta_{max}$ for the N–H resonance was higher than with $H_2PO_4^-$, because of the dianionic form of ATP^{2-}.

In contrast, on complexation of $\mathbf{L_{1-3}}$ with F^- the strongest downfield shifts were observed for the H_α–Cp resonances. For example, with $\mathbf{L_3}$ $\Delta\delta_{max}$ was 0.16 ppm for the α-cyclopentadienyl protons, but was less than 0.01 ppm for the amide protons. Obviously complexation of $\mathbf{L_{1-3}}$ with F^- involves significant interaction between the hard base F^- and the partial positive charge on the iron(II) center in the ferrocene unit, in addition to a weak $N-H\cdots F^-$ hydrogen bonding. Complexation of $\mathbf{L_5}$ with F^- follows the same binding mode, but the amide–fluoride interaction appeared much stronger ($\Delta\delta_{max} = 5.51$ ppm for the amide proton signal) than the Fc–F^- interaction ($\Delta\delta_{max} = 0.48$ ppm for the H_α–Cp protons).

From all these observations, it can be concluded that the strength of the interactions between these neutral ligands and the surveyed anions depends on the number of binding sites contained in the ligands, and on the steric constraints. From $\mathbf{L_1}$ to $\mathbf{L_2}$, and $\mathbf{L_4}$ to $\mathbf{L_5}$ the number of amide groups increases, leading to an enhancement of the hydrogen bonding interactions. However, complexation of F^- and $H_2PO_4^-$ is significantly weaker with $\mathbf{L_3}$ than with the less rigid ligand $\mathbf{L_2}$, both of which contain a 1,1′-bis(amidoferrocene) unit. Accessibility to the binding sites is thus a limiting factor for the strength of the anion–receptor interaction. This point is further highlighted by the behavior of $\mathbf{L_4}$ and $\mathbf{L_5}$ built on the rigid cyclotriveratrylene structural unit. Ligand $\mathbf{L_4}$ contains three amidoferrocene moieties directly bound to the aromatic rings, giving a very rigid structure, which does not allow a favorable organization of the three NH groups. Consequently, $\mathbf{L_4}$ does not present any significant complexation ability in its reduced form towards all the surveyed anions. In contrast, fluoride and dihydrogenphosphate anions interact with $\mathbf{L_5}$, in which the length of the chains linking the ferrocene groups to the cyclotriveratrylene unit was increased by the introduction of additional amide groups, favoring the spatial organization of the binding sites.

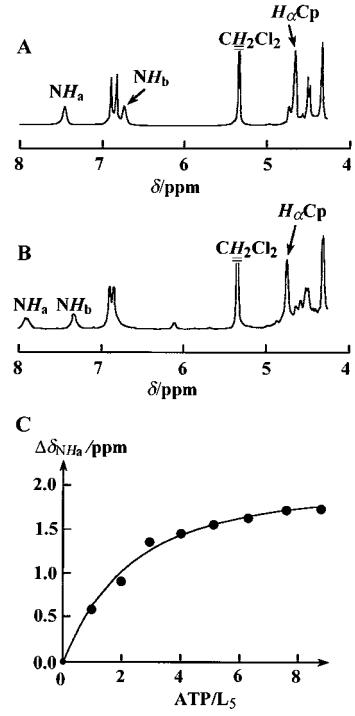

Fig. 1. ^1H NMR spectra of $\mathbf{L_5}$ in CD_2Cl_2. (A) Free $\mathbf{L_5}$; (B) $ATP^{2-}/\mathbf{L_5} = 1$; (C) amide proton shift vs. $ATP^{2-}/\mathbf{L_5}$.

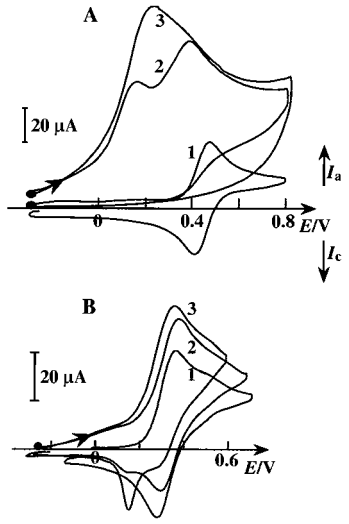

Fig. 2. CVs in CH_3CN + TBAP 0.1 M at a Pt disc (5 mm in diameter) electrode. (A) Curve 1: free $\mathbf{L_3}$; curve 2: $F^-/\mathbf{L_3} = 5$; curve 3: $F^-/\mathbf{L_3} = 10$. (B) Curve 1: free $\mathbf{L_4}$; curve 2: $F^-/\mathbf{L_4} = 1.5$; curve 3: $F^-/\mathbf{L_4} = 2$. Scan rate: 0.1 V s^{-1}.

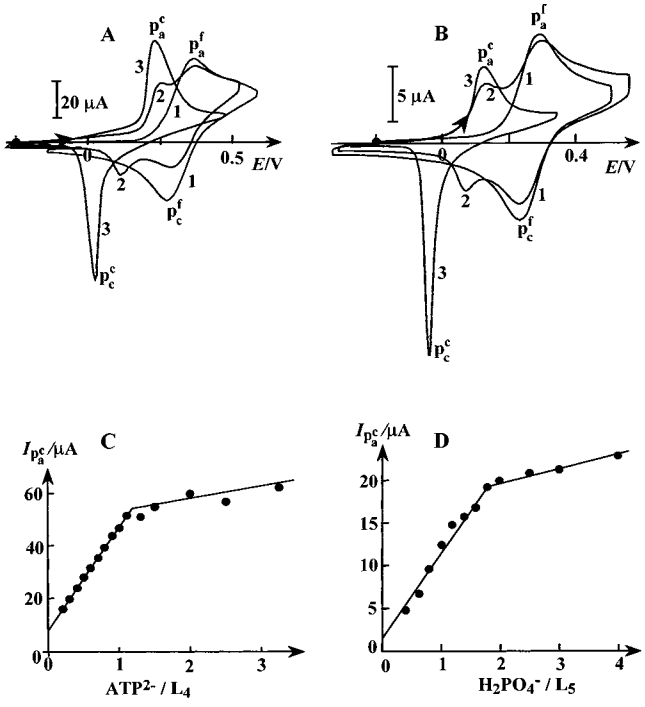

Fig. 3. (A,B) CVs in CH_3CN + TBAP 0.1 M at $v = 0.1$ V s^{-1}. (A) Curve 1: free $\mathbf{L_4}$; curve 2: $ATP^{2-}/\mathbf{L_4} = 0.6$; curve 3: $ATP^{2-}/\mathbf{L_4} = 1$; Pt disc (5 mm in diameter) electrode. (B) Curve 1: free $\mathbf{L_5}$; curve 2: $H_2PO_4^{2-}/\mathbf{L_5} = 1$; curve 3: $H_2PO_4^-/\mathbf{L_5} = 2.2$; carbon disc (3 mm in diameter) electrode. (C,D) Oxidation peak current (I_{pa}^c) vs. anion **L** ratio for the complexed ligand: (C) $\mathbf{L_4} + ATP^{2-}$; (D) $\mathbf{L_5} + H_2PO_4^{2-}$.

Further, the same association constant value was found for $\mathbf{L_5} + H_2PO_4^-$ in CD_3CN and in CD_2Cl_2 (90 M^{-1}), suggesting that the polarity of the solvent does not markedly affect the strength of the H-bond. It should be noted however that the stability constant values of the complexes formed between $\mathbf{L_2}$ and chloride or carboxylate anions were markedly higher in acetone than in dichloromethane [22]. This was attributed to a competition between the solvent and the receptor for binding and solvation of these anions.

3.2. Electrochemical recognition of anions

The electrochemical behavior of the ferrocene derivatives $\mathbf{L_{1-5}}$ has been investigated by cyclic voltammetry (CV) in CH_3CN and CH_2Cl_2 containing 0.1 M tetra-*n*-butylammonium perchlorate (TBAP). The CV curves for $\mathbf{L_{1-5}}$ exhibit the regular wave corresponding to the reversible ferrocene/ferricinium (Fc/Fc^+) redox couple (see, e.g. curve 1 Figs. 2 and 3). Compared with the simple unsubstituted ferrocene, $E_{1/2}$s for $\mathbf{L_{1-5}}$ are shifted towards more positive potentials (Table 2) owing to the substitution of the Cp rings with electron-withdrawing carboxamide groups. It is noteworthy that oxidation of the three Fc centers in $\mathbf{L_4}$ or $\mathbf{L_5}$ occur at the same potential in each ligand, leading to the observation of a single three-electron oxidation wave. This suggests that the three ferrocene groups are not electronically coupled in $\mathbf{L_4}$ and $\mathbf{L_5}$. Moreover, owing to different solvation effects in CH_3CN and CH_2Cl_2 small shifts in $E_{1/2}$s ranging from -40 mV ($\mathbf{L_4}$) to $+80$ mV ($\mathbf{L_2}$) have been observed depending on the solvent used.

The CV behavior of $\mathbf{L_{1-5}}$ is changed in the presence of F^-, HSO_4^-, $H_2PO_4^-$ and ATP^{2-}, according to the receptor–anion couple considered. From a general point of view, two different types of CV behavior for the Fc center in $\mathbf{L_{1-5}}$ have been observed on the addition of increasing amounts of a given anion: (i) a gradual negative shift in the Fc/Fc^+ redox potential (one-wave behavior); or (ii) the growth at a less positive potential of a new redox wave (two-wave behavior) at the expense of the original wave for the free ligand. Negative shifts in the $E_{1/2}$ values on the addition of a guest anion are owing to ion-pairing interactions between the anion and the oxidized, positively charged ligand leading to the stabilization of ferricinium moieties in $\mathbf{L_{1-5}}$. The two-wave behavior is linked to a very strong increase in the anion–ligand interaction following the oxidation of the ligand. This point will be discussed further. During redox cycling, ion-pairing associations are accompanied by adsorption phenomena owing to the weak solubility of the ion pairs in CH_3CN and CH_2Cl_2 electrolyte. This is revealed in the CV curves by a loss of reversibility of the Fc/Fc^+ redox wave, accompanied by the rise of a broad shoulder at the negative foot of the oxidation peak, or by the appearance of a sharp negative stripping peak corresponding to the electroreductive desorption of ion pairs adsorbed on the electrode surface in the oxidation step.

Table 2 summarizes the potential shifts measured in the presence of one molar equivalent of anions. Ac-

cording to the electrochemical features, i.e. a one- or two-wave CV behavior, potential shifts correspond either to the difference between positive peak potentials (ΔE_{pa}), or half-wave potentials ($\Delta E_{1/2}$) for free and complexed ligands.

3.2.1. Electrochemical response to F^-

The electrochemical response for $\mathbf{L_{1-5}}$ in CH_3CN electrolyte is affected by the addition of increasing amounts of fluoride anion. Typical CV curves for $\mathbf{L_3}$ and $\mathbf{L_4}$ are presented in Fig. 2.

With $\mathbf{L_{1-3}}$, a shoulder is seen at the negative foot of the oxidation peak, along with a decrease in the reversibility of the original Fc/Fc^+ wave and with a significant increase in the positive peak current (Fig. 2A, curve 2). The electrochemical response becomes fully irreversible and the shoulder reaches full development when more than two molar equivalents of F^- have been added (Fig. 2A, curve 3). It should be noted that the original oxidation peak is always seen in the CV curves, even in the presence of a large excess of fluoride anion. This behavior is characteristic of an EC mechanism with product adsorption [23], suggesting that oxidized, positively charged $\mathbf{L_{1-3}^+}$ ligands form with F^- insoluble ion pairs that remain strongly adsorbed onto the electrode surface and cannot be reduced in the reverse scan. Thus, the absence of reduction peak in the presence of an excess of fluoride anions can be explained by the very poor solubility of both the $\mathbf{L}^+ + F^-$ ion pair and the $\mathbf{L} + F^-$ complex.

The electrochemical response of $\mathbf{L_4}$ (Fig. 2B) and $\mathbf{L_5}$ to F^- is different from that for $\mathbf{L_{1-3}}$, but can also be explained in terms of ion-pairing association between the ferricinium cation and the fluoride anion. The addition of a slight excess of F^- (e.g. 1.5 molar equivalent) induces the rise of a new negative peak at a less positive potential than the original reduction wave (Fig. 2B, curve 2). This reduction peak becomes sharper at higher $F^-/\mathbf{L}$ ratios (Fig. 2B, curve 3). This stripping peak is owing to the reduction and desorption of ion pairs that precipitate onto the electrode surface during the positive scan. Obviously $\mathbf{L_{1-3}^{3+}} + F^-$ species are more soluble than those formed with $\mathbf{L_{1-3}^+}$. However, the CV wave becomes more and more irreversible in the presence of a large excess of fluoride anions, which favors the formation of weakly soluble $\mathbf{L} + F^-$ complex species and inhibits the dissolution of the ion-pair coating on reduction. On the whole, the CV curves for $\mathbf{L_4}$ and $\mathbf{L_5} + F^-$ present a ill-behaved two-wave behavior, with poorly separated 'free' and 'complexed' positive peaks and adsorption phenomena. These features preclude any accurate amperometric sensing of F^- with $\mathbf{L_4}$ and $\mathbf{L_5}$.

3.2.2. Electrochemical response to $H_2PO_4^-$ and ATP^{2-}

Ion-pairing interactions and adsorption phenomena also mainly govern the electrochemical response in the CH_3CN electrolyte of $\mathbf{L_{1-5}}$ in the presence of dihydrogenphosphate anions. For $\mathbf{L_{1-3}}$ the CV behavior is close to that observed with F^-, and is characterized by the growth of a shoulder at the negative foot of the oxidation peak and by a loss of reversibility in the Fc/Fc^+ redox wave. The larger potential shifts were obtained with $\mathbf{L_1}$ and $\mathbf{L_2}$ (Table 2), and maximum perturbations were observed at anion–ligand molar ratios greater than 2 ($\mathbf{L} = \mathbf{L_2}$), 3 ($\mathbf{L} = \mathbf{L_1}$) and 5 ($\mathbf{L} = \mathbf{L_3}$). These observations show that the interaction between $H_2PO_4^-$ and the rigid $\mathbf{L_3}$ ligand is lower than with $\mathbf{L_1}$ and $\mathbf{L_2}$. The same trend has been found with $\mathbf{L_{1-3}}$ and ATP^{2-}. The CV curves seem to present a two-wave behavior, especially in the case of $\mathbf{L_1}$ and $\mathbf{L_3}$. However, oxidation peaks appeared broad and ill defined, which did not allow the determination of $E_{1/2}$s for the complexed ligands.

In contrast, a clear two-wave behavior was obtained when considering the $\mathbf{L_{4,5}} + H_2PO_4^-$ or ATP^{2-} systems.

Table 2
Electrochemical data[a] for free $\mathbf{L_{1-5}}$, and in the presence of one molar equivalent of guest anions

	Free ligand		F^-		$H_2PO_4^-$		ATP^{2-}		HSO_4^-	
	$E_{1/2}$ (V)		ΔE (V)[b]		ΔE (V)		ΔE (V)[c]		ΔE (V)[b]	
	CH_3CN	CH_2Cl_2	CH_3CN	CH_2Cl_2	CH_3CN	CH_2Cl_2	CH_3CN	CH_2Cl_2	CH_3CN	CH_2Cl_2
$\mathbf{L_1}$	0.28	0.35	−0.22	−0.31	−0.21[b]	−0.17[b]	−0.15	−0.16	−0.005	−0.01
$\mathbf{L_2}$	0.45	0.53	−0.09	−0.29	−0.21[b]	−0.09[b]	−0.14	−0.26	−0.005	−0.02
$\mathbf{L_3}$	0.45	0.50	−0.23	[d]	−0.01[b]	[d]	−0.12	[d]	[e]	[d]
$\mathbf{L_4}$	0.33	0.29	−0.06	[e]	−0.14[c]	−0.23[c]	−0.16	−0.23	[e]	−0.02
$\mathbf{L_5}$	0.28	[d]	−0.09	[d]	−0.17[c]	[d]	−0.16	[d]	[e]	[d]

[a] Versus Ag–$AgNO_3$ 10 mM + TBAP 0.1 M in CH_3CN at $v = 0.1$ V s^{-1}; $A^- = F^-$, $H_2PO_4^-$, ATP^{2-}, HSO_4^-.
[b] $\Delta E = E_{pa}$ ($[A^-] \neq 0$) $- E_{pa}([A^-] = 0)$; one-wave behavior.
[c] $\Delta E = E_{1/2}$ ($[A^-] \neq 0$) $- E_{1/2}([A^-] = 0)$; two-wave behavior.
[d] Not studied.
[e] No significant variation in the electrochemical response.

Typical CV curves are shown in Fig. 3A and B. A well-behaved redox peak system grows at $E_{1/2} = 0.19$ V for $\mathbf{L_4} + H_2PO_4^-$, 0.17 V for $\mathbf{L_4} + ATP^{2-}$, 0.11 V for $\mathbf{L_5} + H_2PO_4^-$, and 0.12 V for $\mathbf{L_5} + ATP^{2-}$ (Table 2). This wave reaches full development at anion–**L** molar ratios close to 2 in the presence of the dihydrogenphosphate anion (Fig. 3D). Maximum perturbation of the CV curves for $\mathbf{L_4}$ and $\mathbf{L_5}$ is obtained with 1 and 1.6 equivalent of the ATP^{2-} dianion added, respectively. This last result is not surprising, taking into account that Fc centers are less sterically hindered in $\mathbf{L_5}$ than in $\mathbf{L_4}$. In these experimental conditions, the original wave for the free Fc/Fc^+ redox couple vanishes and the CV curves present the sole electrochemical response of Fc^+-anion species. Ion pairs are adsorbed onto the electrode surface during the anodic scan, and dissolve in the reverse cathodic scan. Adsorption–desorption phenomena are responsible for a peak-to-peak separation greater than the 60 mV theoretical value for a fully reversible system. However, in sub-stoichiometry mixtures the $\mathbf{L_{4,5}} + H_2PO_4^-$ and ATP^{2-} redox systems appear fully reversible, with $\Delta E_p \cong 0.1$ V. This electrochemical behavior allows amperometric titration curve to be drawn by considering, e.g. the intensity of the positive peak I_{pa}^c corresponding to the complexed ligand versus the anion–ligand molar ratio (Fig. 3C and D). I_{pa}^c increases linearly with the amount of anion added to the solution, to reach a constant value. The two-wave behavior can be attributed to a large increase in the association constant (e.g. by several orders of magnitude) [24] on oxidation, owing to the establishment of very strong electrostatic interactions between $H_2PO_4^-$, ATP^{2-} and the triply charged $\mathbf{L}_{4,5}^{3+}$ species.

3.2.3. Electrochemical response to HSO_4^-

The CV behavior of $\mathbf{L_{1-5}}$ in the CH_3CN electrolyte changed slightly in the presence of hydrogensulphate anions (Table 2). Small negative shifts (around 5 mV) in the $E_{1/2}$s of the Fc/Fc^+ center were observed with $\mathbf{L_1}$ and $\mathbf{L_2}$ (one-wave behavior). Further, no significant variation in $E_{1/2}$s could be measured for $\mathbf{L_3}$, $\mathbf{L_4}$ and $\mathbf{L_5}$, even in the presence of a large excess or HSO_4^-. However, the formation of ion pairs between this anion and the oxidized ligands, and their adsorption onto the electrode surface was evidenced by a clear sharpening of the $Fc^+ \rightarrow Fc$ reduction wave, especially in the case of ligands $\mathbf{L_4}$ and $\mathbf{L_5}$ that contain three ferrocene groups.

3.2.4. Solvent effect on the electrochemical recognition behavior

As the electrochemical recognition properties of $\mathbf{L_{1-5}}$ towards anions depend on both the hydrogen bonding complexation and ion-pairing interactions, the polarity of the solvent could play an important role in the recognition ability of these ligands. In the less polar CH_2Cl_2 electrolyte, the CV behavior of $\mathbf{L_{1-5}}$ is quantitatively the same as in CH_3CN. However, in most cases potential shifts are significantly higher in CH_2Cl_2 (Table 2), suggesting an enhancement of anion–ligand interactions. For example, $\Delta E_{1/2}$ for $\mathbf{L_4} + H_2PO_4^-$ is -230 mV in CH_2Cl_2 electrolyte, against -140 mV in CH_3CN solution. We have seen from ^{1}H NMR experiments that the polarity of the solvent has a weak influence on H-bond interactions between the reduced neutral ligands and anions. Thus, it can be assumed that the solvent polarity affects mainly the ion-pairing associations between the oxidized ligands and anions, as electrostatic interactions are reinforced from a polar to a non-polar solvent. In addition, adsorption phenomena owing to the coating of ion pair species onto the electrode surface are stronger in the CH_2Cl_2 electrolyte. Thus, from an electrochemical recognition point of view two opposing effects occur in the CH_2Cl_2 electrolyte: (i) a favorable effect with an increase in oxidized ligand–anion interactions; and (ii) a negative effect owing to an increased adsorption phenomena which leads to more complex voltammograms.

3.3. Discussion

Comparison between results obtained with $\mathbf{L_{1-5}}$ in the presence of various anions highlights the main parameters that govern anion sensing properties of ferrocene–amide receptors in organic electrolytes. The number of binding sites and ferrocene groups in the receptor, and its topology determine the electrochemical recognition behavior. Interactions between the surveyed anions and receptors $\mathbf{L_{1-5}}$ in their reduced neutral state are relatively weak, with K lower than 250 M^{-1} for all the host–guest systems studied (Table 1). ^{1}H NMR experiments have shown that complexation is mainly owing to H-bonding of anions to amide protons. In the case of the fluoride anion, additional hard base–hard acid interactions with the iron center in the ferrocene group could also be involved. Strong electrostatic interactions are switched on upon the oxidation of ferrocene to ferricinium, especially with $\mathbf{L_4}$ and $\mathbf{L_5}$, which contain three ferrocene groups and show a remarkable two-wave behavior in the presence of $H_2PO_4^-$ and ATP^{2-} anions. It is noteworthy that even when the association constant between the neutral receptor and the anion is too weak to be accessible by ^{1}H NMR studies (e.g. $\mathbf{L_4} + H_2PO_4^-$), the redox ligand is able to recognize the guest anion electrochemically. It can thus be assumed that the oxidation of ferrocene in the vicinity of amide groups increases the acidity of the amide protons and makes hydrogen bonding stronger [25], leading to a synergy between ion pairing and H-bond interactions. Thus, the recognition behavior can be explained in terms of H-bonding complexation, and the magnitude of the electrochemical sensing is

essentially dependent on the strength of ion-pairing interactions. It is not surprising that the best results have been obtained with receptors $\mathbf{L_4}$ and $\mathbf{L_5}$, which contain three and six amide binding sites, respectively, and three ferrocene groups in close proximity. Although the anion–ligand interactions in the reduced state are stronger with $\mathbf{L_5}$ than with $\mathbf{L_4}$, their recognition properties towards F^-, $H_2PO_4^-$ and ATP^{2-} are very close.

The shape of the receptor also has an important effect on the complexation and recognition properties. For example, the association of F^- and $H_2PO_4^-$ with neutral $\mathbf{L_2}$ is stronger than with $\mathbf{L_3}$, while both contain one ferrocene unit and two amide groups. This is likely to be because of the open shape of the binding site in $\mathbf{L_3}$. However, both ligands exhibit very close electrochemical recognition properties, although maximal perturbations in the CV curves are reached at higher anion–ligand ratios with $\mathbf{L_3}$ than with $\mathbf{L_2}$. In the case of $\mathbf{L_4}$ and $\mathbf{L_5}$, which bear three ferrocene centers in close proximity, repulsive electrostatic interactions and steric hindrance do not allow the binding of three anions per receptor molecule. This is clearly seen in the case of $H_2PO_4^-$, where maximal CV perturbations are reached at anion–ligand molar ratios around 2. Further, only one dianionic ATP^{2-} can be bound by ion-pairing association to $\mathbf{L_4}^{3+}$. With $\mathbf{L_5}^{3+}$ this ratio is slightly higher (around 1.6), because of its less sterically hindered structure.

Finally, it should be emphasized that the electrochemical recognition properties of $\mathbf{L_4}$ and $\mathbf{L_5}$ towards the dihydrogenphosphate anion are as important as that reported earlier for dendrimers containing at least nine amido–ferrocene moieties [15]. This comparison shows that the cyclotriveratrylene unit provides an appropriate structural effect in the construction of ferrocene-containing receptors able to sense dihydrogenphosphate and ATP anions in organic electrolytes. It has been shown that cyclotriveratrylene platforms with cationic Ru(arene) [26] or CpFe(arene) [27] pendant arms are good candidates for anion recognition. The new hosts $\mathbf{L_{4,5}}$ thus benefit from the preorganization of the cyclotriveratrylene platform with the three metal centers and NH amide binding sites.

4. Conclusion

This study emphasizes the required parameters for an efficient electrochemical recognition of small anions with ferrocenyl ligands. Significant CV perturbations in the presence of anions were found with mono-ferrocenyl ligands containing one ($\mathbf{L_1}$) or two ($\mathbf{L_2}$, $\mathbf{L_3}$) amide groups, but cannot be used in a simple way to sense anions. Clear CV features, such as a well-behaved two-wave behavior allowing an accurate amperometric titration, require that the redox receptor contain several binding sites and ferrocene groups in close proximity. This goal was achieved with ligands $\mathbf{L_4}$ and $\mathbf{L_5}$ based on the cyclotriveratrylene structural unit.

References

[1] L. Fabbrizzi, A. Poggi, Chem. Soc. Rev. 24 (1995) 197.
[2] P.D. Beer, P.A. Gale, Z. Chen, Adv. Phys. Org. Chem. 31 (1998) 1.
[3] G. Oepen, F. Vögtle, Liebiegs Ann. Chem. (1979) 1094.
[4] A.P. Bell, C.D. Hall, J. Chem. Soc. Chem. Commun. (1980) 163.
[5] T. Saji, Chem. Lett. (1986) 275.
[6] P.D. Beer, Assoc. Chem. Res. 31 (1998) 71.
[7] P.D. Beer, J. Cadman, Coord. Chem. Rev. 205 (2000) 131.
[8] K. Kavallieratos, S. Hwang, R.H. Crabtree, Inorg. Chem. 38 (1999) 5184.
[9] M. Sherer, J.L. Sessler, A. Gebauer, V. Lynch, J. Chem. Soc. Chem. Commun. (1998) 85.
[10] Z. Chen, A.R. Graydon, P.D. Beer, J. Chem. Soc. Faraday Trans. 92 (1996) 97.
[11] A.R. Graydon, P.D. Beer, A.O.M. Johnson, D.K. Smith, Inorg. Chem. 36 (1997) 2112.
[12] J.D. Carr, L. Lambert, D.E. Hibbs, M.B. Hursthouse, K.M. Malik, J.H.R. Tucker, J. Chem. Soc. Chem. Commun. (1997) 1649.
[13] M. Buda, A. Ion, J.-C. Moutet, E. Saint-Aman, R. Ziessel, J. Electroanal. Chem. 469 (1999) 132.
[14] H. Yamamoto, A. Ori, K. Ueda, C. Dusemund, S. Shinkai, J. Chem. Soc. Chem. Commun. (1995) 333.
[15] C. Valerio, J.L. Fillout, J. Ruiz, J. Guitard, J.-C. Blais, D. Astruc, J. Am. Chem. Soc. 119 (1997) 2588.
[16] C.M. Casado, I. Cuadrado, B. Alonso, M. Moran, J. Losada, J. Electroanal. Chem. 463 (1999) 87.
[17] H.-J. Lorkowski, R. Pannier, Z.A. Wende, J. Prakt. Chem. 4 (1967) 141.
[18] J.-C. Moutet, E. Saint-Aman, M. Ungureanu, T. Visan, J. Electroanal. Chem. 410 (1996) 79.
[19] C. Garcia, J. Malthête, A. Collet, Bull. Soc. Chim. Fr. 130 (1993) 93.
[20] G. Vériot, J.-P. Dutasta, G. Matouzenko, A. Collet, Tetrahedron 51 (1995) 389.
[21] KALEIDAGRAPH, Version 3.0.5, Synergy Software (PCS Inc.), Reading, developed by Abelbeck Software Incorporation.
[22] P.D. Beer, M. Shade, J. Chem. Soc. Chem. Commun. (1997) 2377.
[23] R.H. Wopshall, I. Shain, Anal. Chem. 39 (1967) 1514.
[24] S.R. Miller, D.A. Gutowski, Z. Chen, G.W. Gokel, L. Echegoyen, A.E. Kaifer, Anal. Chem. 60 (1988) 2021.
[25] J.D. Carr, S.J. Coles, M.B. Hursthouse, M.E. Light, J.H.R. Tucker, J. Westwood, Angew. Chem. Int. Ed. 39 (2000) 3296.
[26] J.L. Atwood, K.T. Holman, J.W. Steed, J. Chem. Soc. Chem. Commun. (1996) 1401.
[27] K.T. Holman, G.W. Orr, J.W. Steed, J.L. Atwood, J. Chem. Soc. Chem. Commun. (1998) 2109.